Exploring the causal Minkowski-like spaces of observer ensembles and their relational event universes

Oded Shor PhD,[1,3 #] * & Felix Benninger MD[1,2,3 #] & Andrei Khrennikov, PhD[4]

[1]Felsenstein Medical Research Centre, Petach Tikva, Israel; [2]Department of Neurology, Rabin Medical Centre, Petach Tikva, Israel; [3]Sackler Faculty of Medicine, Tel Aviv University, Tel Aviv, Israel; [4]Faculty of Technology, Department of Mathematics, Linnaeus University, Vaxjö, Sweden

Corresponding author (*):

Oded Shor, Felsenstein Medical Research Centre, Petach Tikva, Israel;
shor.oded@gmail.com

 # Equally contributing first authors

Email of all authors:

Oded Shor	shor.oded@gmail.com
Felix Benninger	benninger@tauex.tau.ac.il
Andrei Khrennikov	Andrei.khrennikov@lnu.se

Running title: Exploring causal Minkowski-like spaces of observers ensemble and their relational event universes

Keywords: p-adic numbers; dendrograms; dendrogramic holographic theory; casual structure; Minkowski space; event-universe.

Ethical Publication Statement

We confirm that we have read the Journal's position on issues involved in ethical publication and affirm that this report is consistent with those guidelines.

Funding

This research did not receive any specific grant from funding agencies in the public, commercial, or not-for-profit sectors.

Availability of Data and Materials

No data was gathered or produced in the current study.

Conflicts of Interest

https://doi.org/10.32388/MMVEOF

None of the authors has any conflict of interest to disclose.

Acknowledgements: Chana and Shlomo Chane-Laskin, Eliyahu Myara for intelligent discussion and support.

Abstract. This paper is devoted to event-observational modelling in physics and more generally natural science. The basic entities of such modelling are events and where space-time is the secondary structure for the representation of events. The novelty of our approach is in using a new mathematical picture of events universe. The events observed by an observer are described by a dendrogram, a finite tree. The event dynamics are realized in the dendrogramic configuration space. In a dendrogram, all events are intercoupled via the hierarchic relational structure of the tree. This approach is called Dendrogramic Holographic Theory (DHT). We introduce the causal structure on the dendrogramic space, like the causal structure on the Minkowski space-time. In contrast to the latter, DHT-emergent causality is of a statistical nature. Each dendrogram represents an ensemble of observers with the same relational tree representation of the events they measured/collected. Technically the essence of causal modelling is in encoding dendrograms by real parameters and in this way transitioning to the real space-time. Then we proceed in the framework of information geometry corresponding to Hellinger distance and introduce a kind of light cone in the space of dendrograms. This is a step towards the development of DHT-analog special relativity.

1. Introduction

1.1 Dendrogram representation of events-preliminaries

To achieve our objectives, we employ the following procedure to generate a dendrogram and a dendrogram branch 2-adic expansion.

In our approach, we depict events (referred to as Bohr's phenomena) as branches within a dendrogram, which is essentially a finite tree. Figure 1 provides an illustration that describes the construction of a dendrogramic tree from data. These finite trees serve as an observer's epistemic representation of reality and are constructed as follows:

1. Data collection: Measurements are performed to gather the necessary data.
2. Hierarchical clustering algorithm: A hierarchical clustering algorithm is applied, utilizing a chosen distance metric and a specific clustering (linkage function) algorithm.
3. Agglomerative hierarchical cluster tree: Using the selected distance metric and clustering algorithm, an agglomerative hierarchical cluster tree is constructed. Each event, with its unique branch, can be represented by a binary string or a p-adic expansion of yes/no questions.
4. Dendrogram representation: The set of branches in the tree (or the strings that fully describe them) forms the dendrogram. Each branch, corresponding to a measured event, extends from the root to a leaf (referred to as an edge).

5. Relation between events: A longer common path from root to leaf of two branches signifies a closer relation between the corresponding events, based on the chosen distance metric and clustering algorithm.

Within the context of an infinite number of events, the ontic description of the event-universe is portrayed as an infinite tree. One class of such trees is p-adic trees, which are homogeneous trees with p > 1 edges branching from each vertex. These trees possess an algebraic structure and a topology consistent with this structure. The p-adic topology is governed by the p-adic ultrametric, satisfying the strong triangle inequality. The p-adic distance between two branches of the tree is determined by their common root, where a longer common root signifies a shorter distance. As branches represent events, the space of events, whether finite or infinite, is equipped with a p-adic ultrametric. Therefore, dendrograms encode hierarchic relations between events based on p-adic distances, rather than space-time localization of events. This common root distance determines the level of similarity between events. The geometry of this field exhibits peculiar properties, such as all triangles being isosceles, which arise from the strong triangle inequality. Moreover, upon defining "open" and "closed" balls as

B(R, a) = { x: rp(a, x) <= R} and B-(R, a) = { x: rp(a, x) }

each dendrogram edge can be represented by a 2-adic number:

$edge_i = \sum_{j=0}^{k} a_j \times 2^j$, where $a_j = 0,1$.

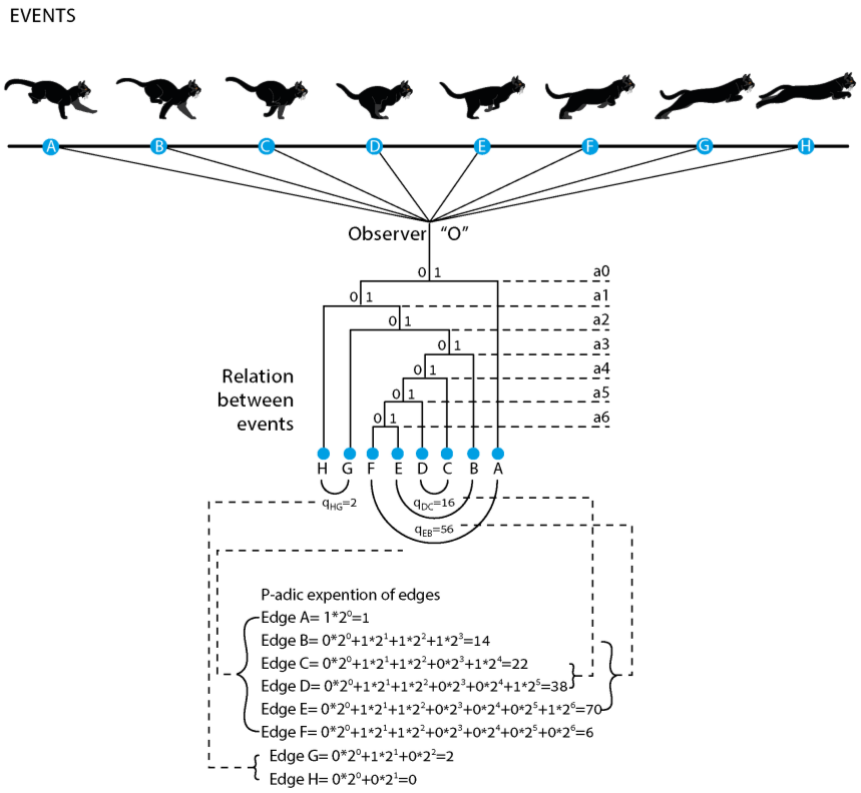

Figure 1.
Relational observation of events. Observer O discriminates events A–H and constructs an object, a dendrogram, which describes the relations between these events. (**B**) Each edge of the dendrogram is a binary string of 0s and 1s which can be represented as a finite p-adic expansion. Each edge summation of its finite p-adic expansion results in a natural number. Subtracting between two edges' finite p-adic expansion results in a "potential gap"—qij.

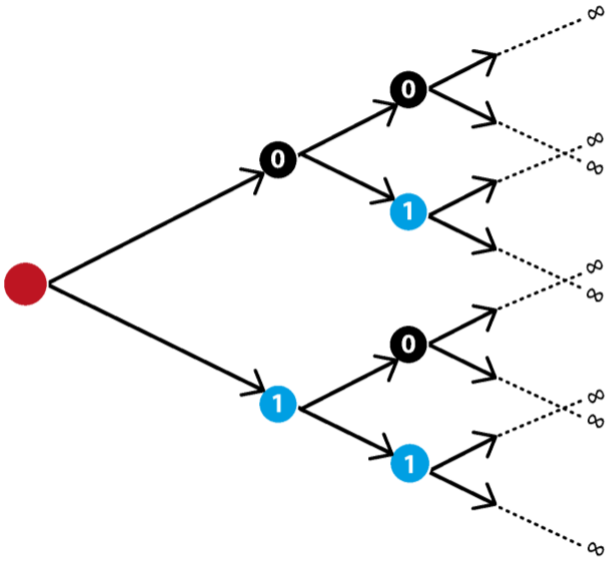

Figure 2. The 2-adic tree

1.2 dendrogramic holographic theory (DHT)

Following the line of papers [1–6], we develop the event-observational approach to physics and more generally natural science [7,8]. In this approach events are the basic entities and where space-time is the secondary mathematical structure explored by observers for the special representation of events. As well as, e.g., in the event (relational) mechanics [3], events are connected via some relational structure. The novelty of our studies is in employing the hierarchic relational structures leading to the representation of events by the branches of trees – *dendrograms*. Finite trees encode the experimental data collected by observers (epistemic dendrograms) and infinite trees represent event-reality as it is (ontic dendrograms). The universe is pictured as an infinite tree covering all possible dendrograms. Depending on the structure of the universal dendrograms, we can consider a variety of possible universes. This approach to event-observational physics (and generally natural science) was structured within the *Dendrogramic Holographic Theory* (DHT) [1–6]. Here the universal tree can be treated as a relational dendrogram.

DHT is not just an abstract theoretical construction. It is directly coupled to the experiment: the experimental data of any origin is transferred into a dendrogram with the aid of clustering algorithms. Temporal dynamics of data collection by an observer are represented as dynamics in the configuration space of dendrograms (see articles [1–3,7,8] for handling concrete experimental data within DHT, especially article [4] devoted to the dynamics). This is a good place to remark that DHT is “invariant to using of different clustering algorithms’’, in the sense that general properties of dynamics do not depend on an

algorithm (although dendrogramic picturing can differ). For simplicity, we proceed with 2-adic, yes-no, clustering algorithms generating homogeneous 2-adic trees, with one incoming and two leaving branches for each vertex. We note that homogeneous trees can be endowed with algebra leading to the number field (or ring) structure. In this way, DHT is connected to the p-adic analysis and theoretical physics [9–14] (including studies of Parisi et al [15] on complex disordered systems). General trees are endowed with ultrametric topology, and such topological spaces were widely used in the theory of complex disordered systems [14,15].

In this paper, we introduce the causal structure on the dendrogramic configuration space, similar to the causal structure on Minkowski space-time. However, in contrast to the latter, DHT-emergent causality is of a statistical nature. So, this is causality on the dendrogramic parameter space where each point in this parameter space represents an ensemble of observers with the same epistemic dendrogramic, relational, representation of the events they measured/collected. We emphasize that the same dendrogram structure can be obtained for a variety of measurement data. In fact, different measurement data sets produce the same epistemic description of the universe when the relations between measurements are the same for different measurement data sets. on the dendrogramic configuration space. In DHT, each observer generates his own event-dendrograms evolving in the configuration space. The transition from one point-dendrogram to another is also observer-dependent. So, the DHT-causal structure is determined by ensembles of observers. In this way, we introduce the timelike and spacelike separated event-dendrograms.

Technically the essence of the causal modelling is in encoding dendrograms by real parameters and in this way transition to the real space-time, i.e., in complete accordance with event mechanics, events are primary, and space-time is secondary.

Following the construction of the dendrogramic parameter space we can introduce the information geometry casual structure. Thus, we consider the information metric on the space of probability distributions based on the Hellinger distance. This information metric determines a dendrogramic “light cone”, which draws an analogy to the Minkowski spacetime metric that characterizes events. This concept allows us to analyze the propagation of information and observer interactions within the dendrogramic framework.

In this paper we perform an extended numerical simulation to check the matching of the dendrogramic and real space representations as well as matching the corresponding notions of causality: in the dendrogramic space and four-dimensional Minkowski space-time.

We emphasize that DHT describes any kind of dynamics of experimental statistical data in the process of collection of outcomes of new observations performed by all possible observers. And it is surprising that any such process can be portrayed in the Minkowski space-time and its causal structure is consistent with the causal structure of special relativity.

2. Causal structure on the space of dendrograms corresponding to ensembles of observables

In our model, we introduce O_i $i=1, 2,\ldots N\to\infty$ observers who collect/measure events/data. Thus, an observer with already collected m events e_1, $e_2\ldots$ e_m collects each time a single event, e_{m+1} Each time an observer O_i collects/measures an event, they construct a dendrogram using the following procedure: Initially, they create a pairwise distance matrix, between all

m+1 events/data collected, where the distance between two acquired events is determined by a pre-defined distance metric. Then, employing a specific pre-chosen clustering algorithm, they construct an agglomerative hierarchical cluster tree, which we refer to as a dendrogram. To represent the dendrogram, we utilize a series of p-adic numbers, with each number encoding the relationship of a single event to the remaining events acquired by the observers. It's important to note that a dendrogram can only be constructed when the number of events is greater or equal to 2, as it relies on the relational structure among events. Initially, all N observers have a trivial dendrogram with two branches.

As observers acquire more events, a range of potential dendrograms with three branches emerges. The number of observers (n) that generate a fixed, same, dendrogram can be represented as a fraction out of all observers (N) in our universe n/ N. Basically, n=n(D), where D is a dendrogram. This iterative process allows the observers' dendrograms to evolve event by event, leading to increasingly complex structures. Please refer to Figure 3 for a visual representation.

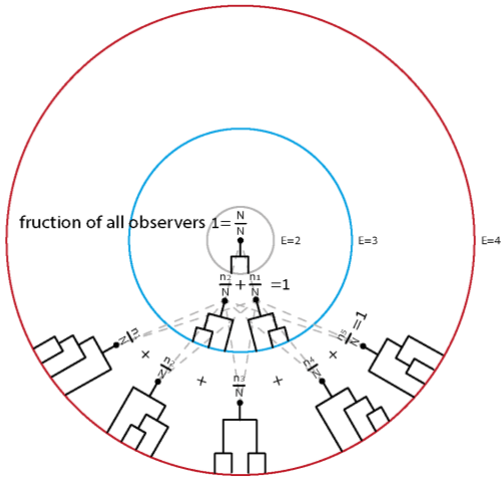

Figure 3. An Abstract Representation of the Dendrogram Space
This figure provides an abstract representation of the dendrogram space. At each level (m=2, 3, ..., M), unique dendrograms are displayed, with each one associated with a specific fraction of the N observers present in the universe. It is noteworthy that the cumulative fraction of observers' dendrograms at each level precisely sums up to 1, illustrating the complete representation of the entire observer population. In each level m=2,3,…M, each unique dendrogram belongs to a fraction of the N observers present in the universe. Each level's total fraction of observers' dendrograms sum to 1

Now, we explore the question of whether a given dendrogram will transfer any fraction of observers from itself to another dendrogram in the future. By examining the structure of two dendrograms, can we predict whether they are connected? Dendrograms that exhibit observer flow from one to the other can be referred to as "timelike separated" dendrograms, while dendrograms that show no observer flow between them can be classified as "spacelike separated". More specifically, "timelike/spacelike separated" dendrograms are defined as follows:

D1 and D2 are two, timelike separated, different dendrograms with the number of events/data collected $e1 \leq e2$*, respectively,*

if and only if there exists at least one observer with D1 dendrogram with $e1$ *events moves from D1 to D2 upon collecting the next* $e2 - e1$ *events*

D1 and D2 are two, spacelike separated, different dendrograms with the number of events/data collected $e1 \leq e2$*, respectively,*

if and only if there is no possibility for observers with D1 dendrogram with $e1$ *events to move from D1 to D2 upon collecting the next* $e2 - e1$ *events*

In essence, we introduce the concept of a dendrogramic "light cone," which draws an analogy to the Minkowski spacetime metric that characterizes events. This concept allows us to analyze the propagation of information and observer interactions within the dendrogramic framework.

By discerning the relationships and connectivity patterns among dendrograms, we aim to gain insights into the causal connections and spatiotemporal dynamics within the observed events. Through this analysis, we can uncover the underlying structures that govern the flow of information and the evolution of the observer's dendrograms.

Please note that while the causal structure of Minkowski space is not statistical in nature, in DHT, we seek to establish a statistical counterpart referred to as the *"dendrogramic Minkowski causal structure of observers ensemble relational universes"*. In this context, each dendrogram represents a fraction of observers who collect a specific number of events (n) this fraction of observers has the same relations between their acquired events.

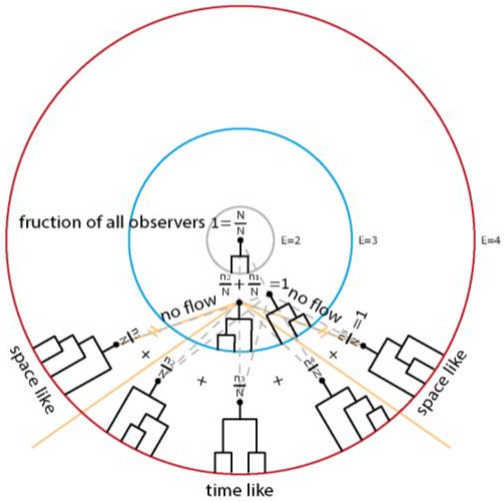

Figure 4. An Abstract Representation of the Causal Structure in the Dendrogram Space

This figure provides an abstract representation of the causal structure within the dendrogram space. Each dendrogram is characterized by a specific number of events, with one dendrogram containing E2 events located inside the light cone of another dendrogram containing E1 events, where E2 is greater than n1. Remarkably, this relationship implies that at least one observer possessing the dendrogram with n1 events can transform it into the dendrogram with E2 events by collecting E2-E1 additional events. The illustration highlights the dynamic nature of the dendrogram space and its potential for causal transformations facilitated by event collection.

In order to achieve this objective, we require a parameter space for dendrograms that uniquely characterizes each individual dendrogram. Remarkably, we demonstrate that such a parameter space can be obtained, and intriguingly, it manifests as a four-dimensional space. Additionally, we observe that the interval between any two dendrograms in this parameter space exhibits a signature akin to Minkowski spacetime—a combination of spacelike intervals with positive values and timelike intervals with negative values, or vice versa.

3. Real parametrization of dendrograms

In our study, we employed the following equation to facilitate our analysis: The representation of a dendrogram branch, denoted as $edge_i$, can be expressed as the sum of a series: $edge_i = \sum_{j=0}^{k} a_j \times 2^j, \quad a_j = 1,0$ *(1)*

where each term corresponds to the contribution of a specific level in the dendrogram's hierarchical structure. Here, a_j represents the binary digit at position j, with possible values of 0 or 1.

To further enhance our analysis, we introduce the concept of the monna map conversion. The monna map conversion of an event, denoted as $event_i$, is computed using the formula: $event_i = \sum_{j=0}^{k} a_j \times 2^{-j-1}$, $a_j = 1,0.$

(2)

where a_j represents the binary digits (0 or 1) in the 2-adic expansion of the dendrogram branch, and k is the maximum ball level of the dendrogram.

By applying this Monna map conversion, we represent events as rational numbers on the continuous interval [0, 1]. This conversion preserves the precise relations between events, ensuring that the inherent structure and ordering within the dendrogram branches are maintained. To quantify the differences between events, we introduced the metric q_{ik}, which represents the absolute difference between the monna map conversions of two events,

$q_{ik} = |event_i - event_k|$ *(3)*

Thus, we can define 5 elementary/fundamental parameters of a dendrogram

We define our dendrogramic vector, D, as follows:

$$E = event_i, i = 1,2 \dots n = number\ of\ events$$

$$B = 2^{-maximal\ ball\ level\ of\ the\ dendrogram}$$

$$D = [E\ B] with\ elements\ D_i, i = 2,3 \dots n+1$$

$$V_D = (\sum_{i=0}^{k} D_i)^z$$

$$U_D = (\sum_{i=0}^{k} \frac{1}{D_i + 1})^{z1}$$

$$M_D = (\sum_{i=1}^{k-1} \sum_{j=i+1}^{k} D_i \cdot D_j)^{z2}$$

$$R_D = (\sum_{i=1}^{k-1} \sum_{j=i+1}^{k} D_i - D_j)^{z3} = (\sum_{i=1}^{k-1} \sum_{j=i+1}^{k} q_{ij}) + \sum_{j=i+1}^{k} |B - D_j|)^{z3}$$

$$r_D = (\sum_{i=1}^{k-1} \sum_{j=i+1}^{k} 1/((D_i - D_j) + 1))^{z4} =$$

$$(\sum_{i=1}^{k-1} \sum_{j=i+1}^{k} 1/(q_{ij} + 1) + \sum_{j=i+1}^{k} 1/(|B - D_j| + 1))^{z4}$$

$k = number\ of\ branches\ and\ thus\ events\ in\ dendrogram$ *(4)*

Where z,z1,z2,z3 and z4 each takes randomly a value from T=[-2 -1 -0.5 0.5 1 2]

We then constructed from a combination of them another 55 parameters in the following way.

1. All possible two elementary parameters product combinations. Thus adding 10 more parameters
2. All possible two elementary parameters sum combinations. Thus adding 10 more parameters
3. All possible two elementary parameters division combinations. Thus adding 20 more parameters
4. All possible three elementary parameters product combinations. Thus adding 10 more parameters
5. All possible four elementary parameters product combinations. Thus adding 5 more parameters.

Overall, we had 60 possible parameters. These 60 parameters were used for a numerical deep scan of possible "dendrogramic Minkowski causal structure of observers ensemble"

4. Establishing dendrogram-parameters coupling via numerical simulation

The problem of encoding dendrograms using real parameters is mathematically challenging and can require a significant amount of time to find a solution. In the context of Data-Driven Hypothesis Testing (DHT) theory, where simulations have provided valuable insights, we propose a method called "numerical experimenting confirmation" to select parameters. Through an extensive numerical simulation, we demonstrate the validity of our real parametrization on the space of dendrograms. While this approach does not provide a mathematical proof, the likelihood of encountering dendrograms that do not conform to our parametrization is practically negligible. As a result, we confidently propose the use of this parametrization for the extended space of dendrograms. In this technical section, we present the output and findings of our numerical simulation.

Process 1 was to determine how many different, unique, dendrograms are possible in some "number of events-level n".

We followed these sub-steps: Here are the sub-steps of the given process:

1. Generate 100,000 vectors of n values (representing events) for each n = 5, 6, and 7.
2. Randomly select n values from the interval [0, 1] for each vector.
3. Compute pairwise Euclidean distances between elements in each vector.
4. Construct agglomerative hierarchical cluster trees using the "single" linkage method for each vector.
5. Identify distinct dendrogram structures for each "number of events-level n".
6. Count the number of different dendrogram structures obtained for each n.

For n=5, we found m=4 different dendrogram structures. For n=6, we obtained m=9 different dendrogram structures, and for n=7, we discovered m=21 different dendrogram structures.

Process 2 we produced 100 "observers" for each of the m=4,9,21 unique and different dendrograms each in its corresponding n=5,6,7 event level.

1. Randomly select n numbers from the interval [0, 1]
2. Construct a dendrogram D out of the n numbers (as in steps 3 and 4 of process 1)
3. Identify to which of the m different dendrograms D equals to.
4. The n random numbers define $Observer_{ij}$ i=1,2,…100 j=1,2….m
4. Repeat until i=100 for all j

Thus, although each of the 100 "observers" collected different n events/numbers their relational observed universe is the same.

Process 3 Producing all possible dendrograms an "observer" can evolve to by adding k=1,2,…6 events.

1. For each "observer" we add k random numbers (k=1-6) t times (t=4000*(1+k/2) for n=5,6. t=6000*(2+k/2) for n=7)
2. Construct a dendrogram D out of the n numbers (as in steps 3 and 4 of process 1).

Overall, in the end, for all 100 observers we produced for all k=1,2,…6 we produced 4*1600000, 9*1600000 and 21*3000000 non-unique dendrograms for n=5,6,7 respectively.

In that way, we could know for a single observer in its initial "events-level n" what are the possible dendrogram that it can transfer to in each of the "events-level n+k"

In each scenario of n+k events, starting from a specific initial dendrogram with n events, we examined the set of possible unique dendrograms that could emerge. This analysis allowed us to determine the distribution of these unique n+k events dendrograms that arise from any of the m's unique initial dendrograms as shown in Figure 5 for n=6.

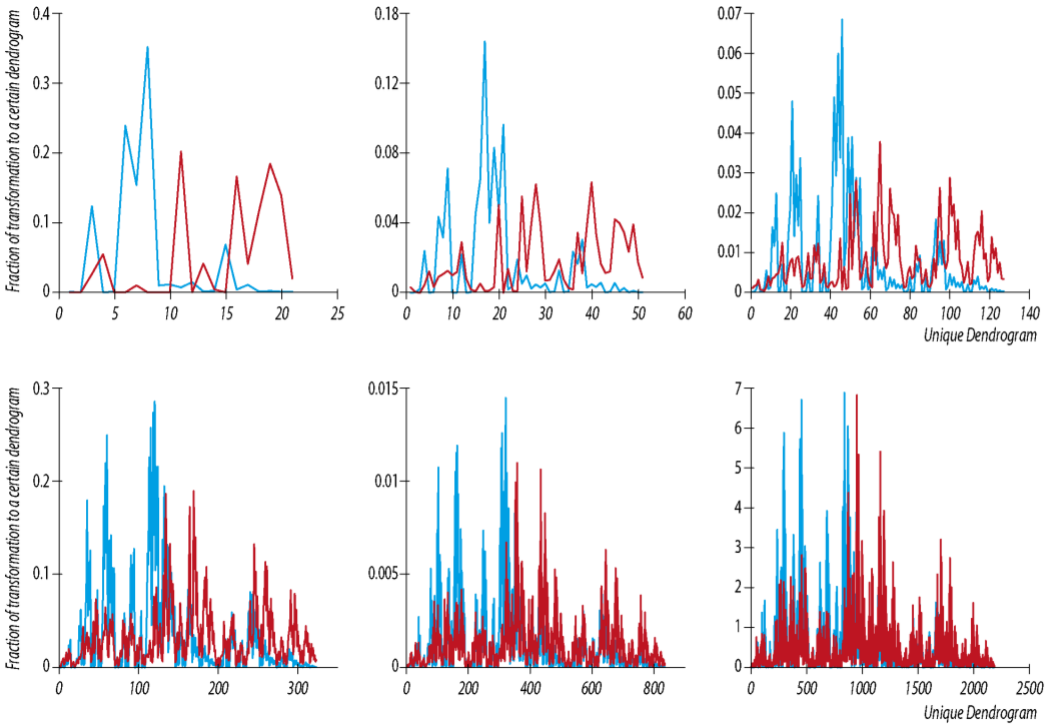

Figure 5. Distribution of Dendrograms at n+k Level for Two Different Initial Dendrograms with 6 Events. This figure illustrates the evolutionary process of two distinct initial dendrograms, namely Dendrogram A and Dendrogram B, each consisting of 6 events. The diagram showcases the distribution of dendrograms that emanate from each initial dendrogram at various n+k levels (k = 1, 2, 3, 4, 5, and 6). At each level, the initial dendrograms undergo transformation and branching, leading to the emergence of unique configurations represented by subsequent dendrogram structures. The visualization offers insights into the dynamic nature of dendrogram evolution as they progress through different levels.

Interestingly, all m dendrograms with n=5 could be transformed to all possible dendrograms at n+k levels where k has the value of 2-6. However, for the m dendrograms with n=6, this encompassing occurred only for n+k levels where k has the value of k=3-4. This implies that some of the m initial dendrograms with n=5 exhibited spacelike dendrograms solely at k=1, whereas for dendrograms with n=6, the presence of spacelike dendrograms varied across different levels. Specifically, the number of initial dendrograms with n=6 that had spacelike dendrograms differed for each level (Figure 6A1-A2).

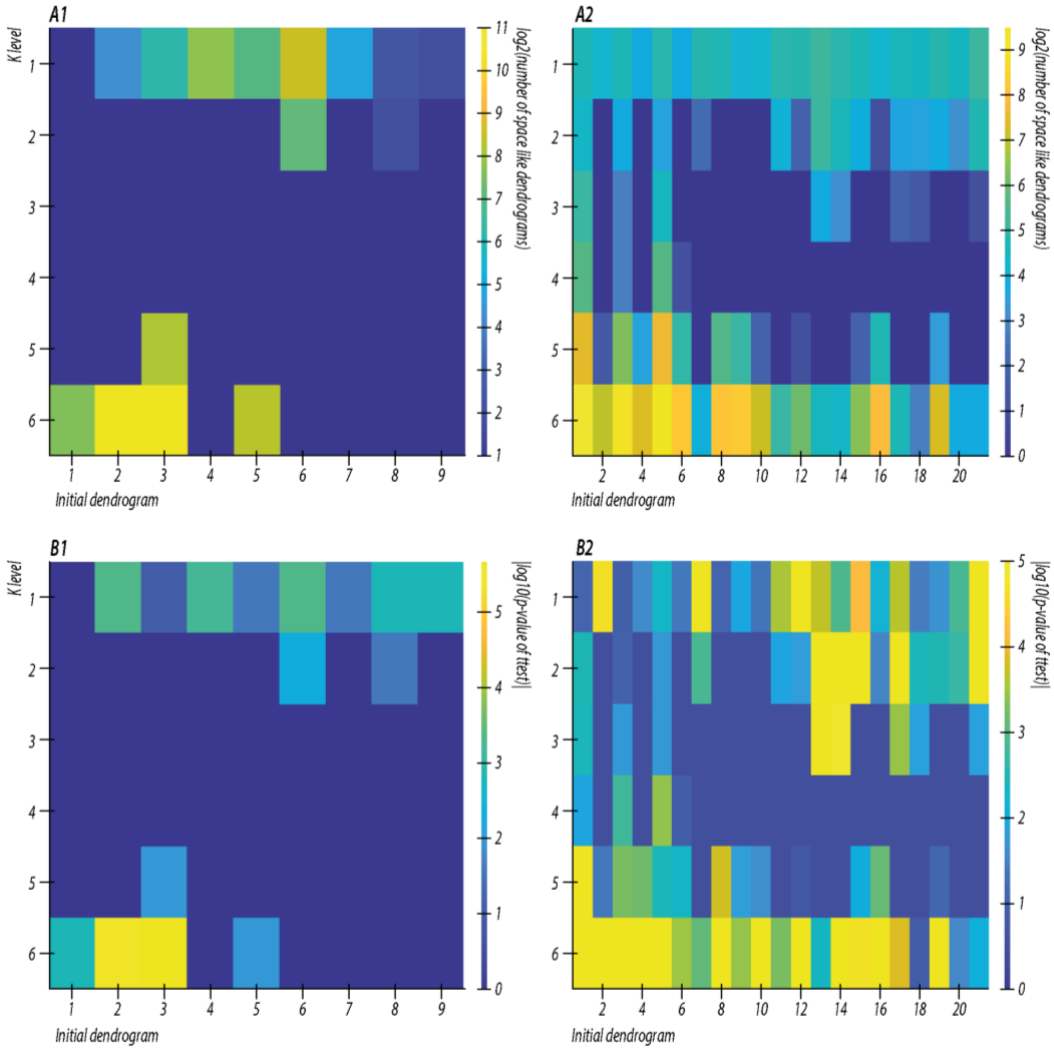

Figure 6. A1 Number of Spacelike Dendrograms for Each k (Initial Level n=6) This subfigure depicts the count of spacelike dendrograms at each k level for various initial dendrograms, all having an initial level of n=6. Each k level demonstrates a distinct number of unique spacelike dendrograms, specifically 21, 51, 127, 323, 835, and 2188, representing different configurations of dendrogram structures. **A2 Number of Spacelike Dendrograms for Each k (Initial Level n=7)** This subfigure displays the count of spacelike dendrograms at each k level for different initial dendrograms, with a shared initial level of n=7. At each k level, there are 51, 127, 323, 835, 2188, and 5798 unique spacelike dendrograms, reflecting diverse configurations of dendrogram structures. **B1 Mean Significance of Intervals in Selected Parameters of Spacelike vs. Timelike Dendrograms (Initial Level n=6)** This subfigure presents the average significance values of intervals within selected parameters for spacelike and timelike dendrograms at each k level, considering various initial dendrograms with an initial level of n=6. The comparison between spacelike and timelike dendrograms allows for an assessment of the significance variations across different intervals in the selected parameters. **B2 Mean Significance of Intervals in Selected Parameters of Spacelike vs. Timelike Dendrograms (Initial Level n=7)** This subfigure exhibits the average significance values of intervals within selected parameters for spacelike and timelike dendrograms at each k level, considering different initial dendrograms with an initial level of n=7. The comparison between spacelike and timelike dendrograms enables an examination of the significance variations across different intervals in the selected parameters.

For each of the m unique initial dendrogram with n events, the resulting n+k level corresponds to a set of unique dendrogram structures. This set can encompass either the complete set of possible unique dendrograms for the n+k level or a partial set, depending on the specific scenario. The case of a set that is a partial subset of all possible unique dendrograms at the n+k level means there are dendrograms that observers with one of the m initial dendrograms do not evolve to ("spacelike" dendrograms relative to the initial n-level unique dendrogram).

These results raise the question of whether we can assign Minkowski-like signatures to these dendrograms, with signatures opposite in sign for dendrograms observers can/cannot evolve to.

Interestingly, the absolute difference between some of the 60 parameter values an initial dendrogram (one of the m possible) and the corresponding dendrograms it evolved to, at some level n+k, showed a significant difference compared to the absolute difference between the parameter values an initial dendrogram (one of the m possible) and its corresponding dendrograms it did not evolve to, at some level n+k.

After performing 5000 iterations of random selection for z, z1, z2, z3, and z4, we identified 23 out of the 60 parameters that exhibited statistical significance ($p < 0.05$ in t-test) in at least 60% of the occurrences where “timelike” and "spacelike" dendrograms both existed for an initial specific m dendrogram. Furthermore, these parameters showed significance in at least 70% of the random selections of z, z1, z2, z3, and z4 (an example is shown in Figure 4 B.1-B.2).

With those selected parameters, we randomly pick a parameter s2 from the set S = [0.5, 1, 1.5, 2, 2.5]. This parameter will take the same role as the speed of light in special relativity. We consider all four possible combinations out of the 23 selected parameters above $\theta_1 , \theta_2 , \theta_3 \; and \; \theta_4$, and for each such combination, we perform the following four calculations:

We take all possible order permutations of the parameter $\theta_1 , \theta_2 , \theta_3 \; and \; \theta_4$

Each such permutation is now based on order $\theta'_1 , \theta'_2 , \theta'_3 \; and \; \theta'_4$ we calculate for the three first parameter

$$INTERVAL_i = (\theta'_{i \; initial \; dendrogram} - \theta'_{i \; n+k \; level \; dendrogram})^2 \; i = 1,2,3$$

And we define n= initial dendrogram number of events

n+k=level of transmitted/not transmitted dendrogram, k=1,2,3,4,5,6. then

$$INTERVAL_4 = (\sqrt{n}\theta'_{i \; initial \; dendrogram} - (\sqrt{n+k})\theta'_{i \; n+k \; level \; dendrogram})^2 \; i = 4$$

(5)

We then calculate the following four quantities:

$$INterval = INTERVAL_1 + INTERVAL_2 + INTERVAL_3 - s2 * INTERVAL_4$$

(6)

We conducted 5000 iterations, exploring various combinations of constants (z, z1, z2, z3, z4, and s2), to identify parameter sets consistently demonstrating opposite sign intervals between timelike and spacelike dendrograms. This analysis encompassed all initial m dendrograms (limited to n=6) and their corresponding spacelike/timelike dendrograms at n+k levels (k=1, 2, ..., 6).

Remarkably, our analysis revealed the existence of parameter spaces with two distinct causality structures: one characterized by a "negative spacelike signature" and the other by a "positive spacelike signature."

In the case of the "negative spacelike signature," we observed that the interval between two spacelike dendrograms was consistently negative. Specifically, the sum of the first three "space" parameters ($INTERVAL_1 + INTERVAL_2 + INTERVAL_3$) was consistently smaller than s2 multiplied by $INTERVAL_4$. This negative signature held true across all intervals computed from the parameters of the 9 initial n=6 level dendrograms and their corresponding n+k spacelike dendrograms (where k ranged from 1 to 6). Notably, the timelike dendrograms derived from each of the n=6 initial dendrograms consistently exhibited positive values for their respective time-like parameter intervals. Importantly, this reversed causality structure was consistently observed across all 9 initial dendrograms and their unique sets of n+k dendrograms (totaling 21, 51, 127, 127, 834, and 2400 such dendrograms for k=1, 2, ..., 6, respectively). This observation contradicts the ordinary causal structure of the real Minkowski metric in special relativity and its resulting characteristic light cone, where information cannot be transmitted between two spacelike separated events for the trivial cause that the sum of the space coordinates' intervals is greater than the distance light can travel within the given time interval.

Conversely, the "positive spacelike signature" aligns with the characteristics of the Minkowski metric. In this scenario, the sum of the first three "space" parameters ($INTERVAL_1 + INTERVAL_2 + INTERVAL_3$) consistently surpasses s2 multiplied by $INTERVAL_4$. 4. Once again, this positive "space like signature" remained consistent for all intervals computed from the parameters of the 9 initial n=6 level dendrograms and their corresponding n+k spacelike dendrograms (with k ranging from 1 to 6). Interestingly, the timelike dendrograms derived from each of the n=6 initial dendrograms consistently exhibited negative values for their respective time-like parameter intervals. It is worth noting that this Minkowski-like causality structure persisted across all 9 initial dendrograms and their unique sets of n+k dendrograms (totaling 21, 51, 127, 127, 834, and 2400 such dendrograms for k=1, 2, ..., 6, respectively).

In our random numerical analysis, we observed a higher occurrence of parameter spaces with a "positive spacelike signature" compared to those with a "negative spacelike signature." Remarkably, each of these two distinct parameter spaces maintained consistency and demonstrated opposite sign intervals between timelike and spacelike dendrograms across all initial n dendrograms (specifically n=6) and their corresponding n+k level dendrograms.

Figure 7 illustrates the overall rather peculiar and counter-intuitive causality, where timelike intervals have positive values and spacelike intervals have negative values. This causality structure aligns with increasing levels of k for the initial dendrogram of n=6 in the time/space-like dendrograms. Figure 8 demonstrates that the overall causality, as indicated by the intervals with a positive spacelike signature, remains consistent with increasing levels of k for initial dendrogram levels n=6 in both the time-like dendrograms and the space-like dendrograms.

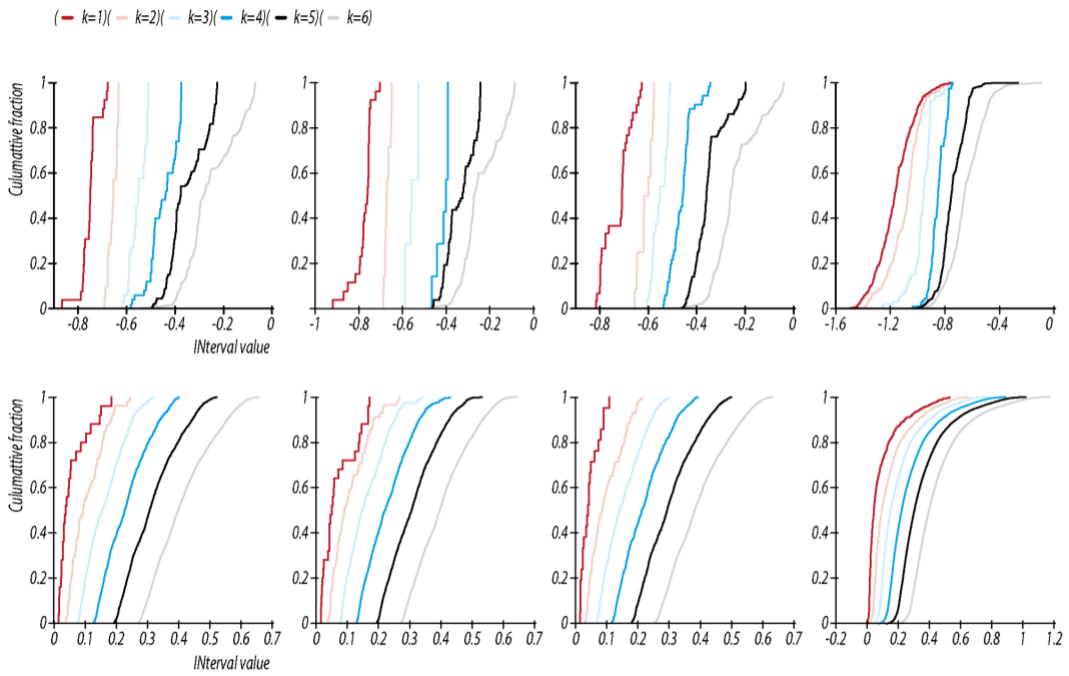

Figure 7. Time-Like and Spacelike Dendrogram Interval Values for the Negative Spacelike Signature Parameter Space

This figure explores the interval values for time-like and spacelike dendrograms in the context of the negative spacelike signature parameter space. The figure is divided into several panels, each representing different aspects of the analysis. **Top row first 3 panels from the left: Cumulative Distribution Functions (cdfs) of Interval Values for Spacelike Dendrograms** depict the cumulative distribution functions (cdfs) of INterval values for spacelike dendrograms, focusing on three specific initial dendrograms at the initial level n=6 and varying k values (k=1, 2, ..., 6). Each panel showcases the distribution of interval values for spacelike dendrograms resulting from the transformation and branching processes. **Top row panel on the right: Cumulative Distribution Function (cdfs) of Interval Values for All Spacelike Dendrograms** presents the cumulative distribution function (cdfs) of INterval values for spacelike dendrograms, encompassing all initial dendrograms at the initial level n=6 and for each k value (k=1, 2, ..., 6). The visualization offers an overall perspective of the interval value distributions across all spacelike dendrograms. **Bottom row first 3 panels from the left: Cumulative Distribution Functions (cdfs) of Interval Values for Time-Like Dendrograms** illustrate the cumulative distribution functions (cdfs) of INterval values for time-like dendrograms, focusing on three specific initial dendrograms at the initial level n=6 and varying k values (k=1, 2, ..., 6). Each panel provides insights into the distribution of interval values for time-like dendrograms resulting from the transformation and branching processes. **Bottom rowrightpanel: Cumulative Distribution Function (cdfs) of Interval Values for All Time-Like Dendrograms** displays the cumulative distribution function (cdfs) of INterval values for time-like dendrograms, encompassing all initial dendrograms at the initial level n=6 and for each k value (k=1, 2, ..., 6). The visualization presents an overall perspective of the INterval value distributions across all time-like dendrograms.

.

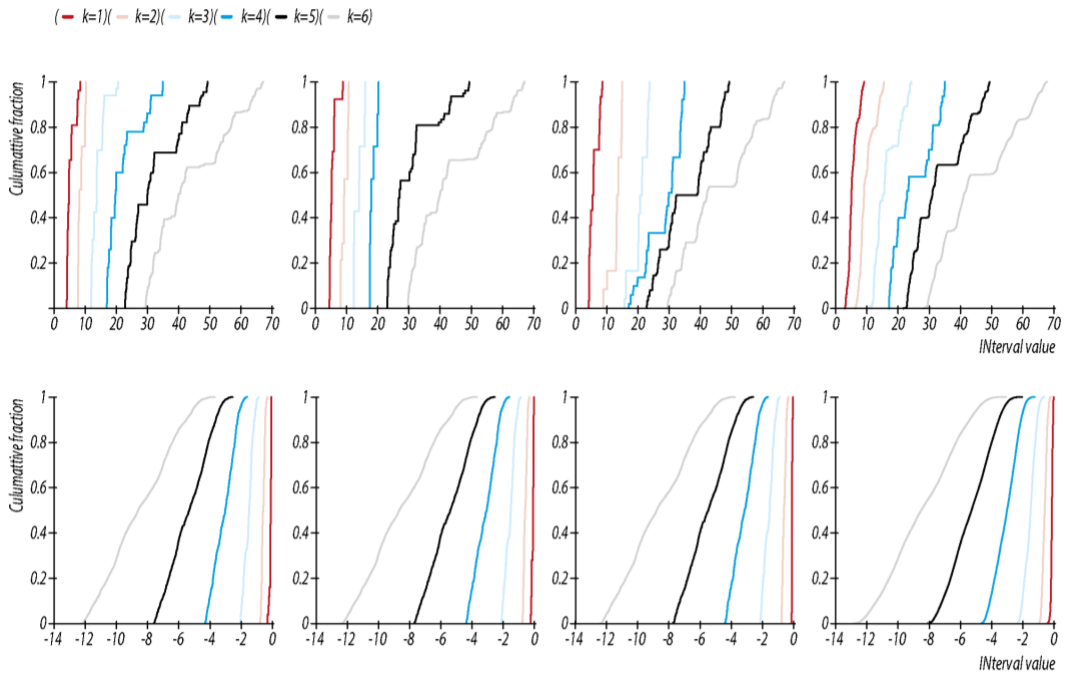

Figure 8. Time-Like and Spacelike Dendrogram Interval Values for the Positive Spacelike Signature Parameter Space This figure explores the interval values for time-like and spacelike dendrograms in the context of the positive spacelike signature parameter space. The figure is divided into several panels, each representing different aspects of the analysis. **Top row first 3 panels from the left: Cumulative Distribution Functions (cdfs) of Interval Values for Spacelike Dendrograms** depict the cumulative distribution functions (cdfs) of INterval values for spacelike dendrograms, focusing on three specific initial dendrograms at the initial level n=6 and varying k values (k=1, 2, ..., 6). Each panel showcases the distribution of interval values for spacelike dendrograms resulting from the transformation and branching processes. **Top row panel on the right: Cumulative Distribution Function (cdfs) of Interval Values for All Spacelike Dendrograms** presents the cumulative distribution function (cdfs) of INterval values for spacelike dendrograms, encompassing all initial dendrograms at the initial level n=6 and for each k value (k=1, 2, ..., 6). The visualization offers an overall perspective of the interval value distributions across all spacelike dendrograms. **Bottom row first 3 panels from the left: Cumulative Distribution Functions (cdfs) of Interval Values for Time-Like Dendrograms** illustrate the cumulative distribution functions (cdfs) of INterval values for time-like dendrograms, focusing on three specific initial dendrograms at the initial level n=6 and varying k values (k=1, 2, ..., 6). Each panel provides insights into the distribution of interval values for time-like dendrograms resulting from the transformation and branching processes. **Bottom row panel on the right: Cumulative Distribution Function (cdfs) of Interval Values for All Time-Like Dendrograms** displays the cumulative distribution function (cdfs) of INterval values for time-like dendrograms, encompassing all initial dendrograms at the initial level n=6 and for each k value (k=1, 2, ..., 6). The visualization presents an overall perspective of the INterval value distributions across all time-like dendrograms.

Out of the 5000 randomly generated combinations of constants (z, z1, z2, z3, z4, and s2), our analysis identified 260 distinct combinations that demonstrated consistency across all n+k levels for the initial set of 9 dendrograms with n=6. This consistency was

defined by the inverse sign between the computed $INterval$ values, as defined in equation 6, for the timelike dendrograms and their corresponding n+k spacelike dendrograms.

Furthermore, we discovered a total of 3117 different combinations of constants (z, z1, z2, z3, z4, s2) and parameters (θ'_1, θ'_2, θ'_3, θ'_4) that exhibited this remarkable consistency. Among these combinations, 797 displayed a "negative spacelike signature," while 2320 exhibited a "positive spacelike signature" (as depicted in Figure 9).

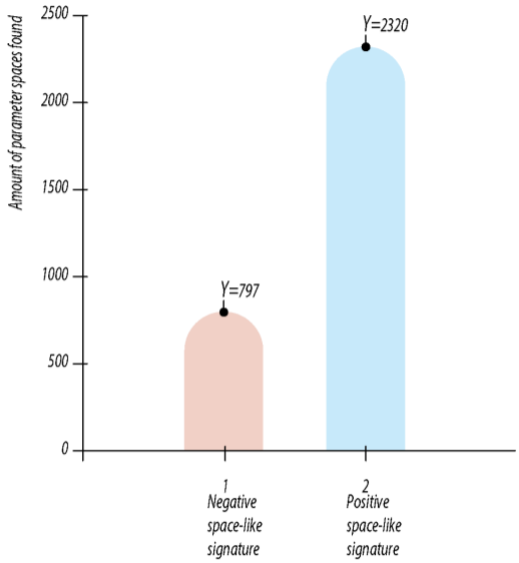

Figure 9. Number of "negative spacelike signature and positive spacelike signature parameter spaces found in our simulations

We then tested the consistency of the found sets of these 3117 parameters and constants in the same way for the initial dendrograms of n=5 and n=7.

We observed that when preparing the dendrogram parameters according to the described method, only specific combinations of θ'_1 , θ'_2 , θ'_3 and θ'_4 can uniquely describe a dendrogram. Such uniqueness is achieved when one of the parameters (θ'_1 , θ'_2 or θ'_3) is either V_D or U_D, and another parameter is a product, sum, or division of the two. Alternatively, when one of the parameters is R_D or r_D, and another parameter is a product, sum, or division of the two.

Interestingly, we discovered that all 797 combinations with a "negative spacelike signature" were unable to uniquely define the dendrogram space. This suggests that in order for a coordinate/parameter space to uniquely define events (or dendrograms in our case), as is the case in ordinary spacetime, it must possess the light cone characteristics and vice versa. In the context of spacetime intervals spacelike intervals are characterized by $\sum \Delta X^2 > c\Delta t^2$ whereas time-like intervals are characterized by $\sum \Delta X^2 < c\Delta t^2$. In these cases with "negative spacelike signature," where this condition was reversed, we lost the unique definition of dendrograms.

Out of the total 2320 consistent parameters that exhibited a "positive spacelike signature," only 310 combinations were found to uniquely define the dendrogram space (refer to Figure 10).

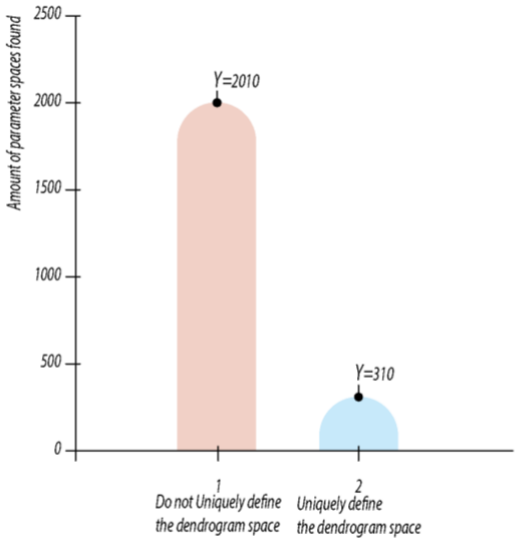

Figure 10. Number of positive spacelike signatures that uniquely define the dendrogram space vs. positive spacelike signatures that did not uniquely define the dendrogram space found in our simulations.

To further investigate this conjecture, we examined a mixture of 760*137 parameter combinations that possessed either a "negative spacelike signature" or a "positive spacelike signature" in n=6 while still being able to uniquely define the dendrogram space. As expected, all the parameters with a "negative spacelike signature" could not exhibit consistent opposite sign values for all its intervals produced from time-like dendrograms compared to all its intervals produced from spacelike dendrograms across all initial n dendrograms (n=5,6,7) and for all their n+k levels dendrograms. Consequently, these parameters failed to maintain the causal structure of the “reversed” non-trivial light cone.

Thus, in cases of parameters exhibiting consistent "negative spacelike signature" with “reversed” causal structure and non-trivial light cone they fail to uniquely define the dendrogram space. while those that do possess the ability to uniquely define the dendrograms space lose the consistency of the casual structure of the “reversed” light cone.

On the other hand, some of the parameter spaces (49 of them) with a "positive spacelike signature" exhibited the necessary consistency of the casual structure of the light cone, in all tests conducted for n=5, 6, and 7 (as described earlier). This outcome confirmed that the only possible casual structure must resemble the ordinary Minkowski metric light cone.

I n order to validate the applicability of the 310 combinations of $\theta'_1, \theta'_2, \theta'_3 \; and \; \theta'_4$ that were both consistent and could uniquely define the dendrogram space we conducted the following test: 20000 times we randomly generated a dendrogram with a random size smaller than 100 events and its corresponding timelike dendrogram, which was obtained by adding random k events to the initial dendrogram. The value of k satisfied the condition;

*number of events in initial dendrogram<k<2*number of events in initial dendrogram*

Among the 20,000 tests conducted on "positive space-like signature spaces," none of the cases yielded positive values, thereby illustrating the consistency of the time-like negative signature. This finding is exemplified in Figure 11.
The consistent overall combinations of z, z1, z2, z3, z4, s2 and θ'_1 , θ'_2 , θ'_3 θ'_4 were kept for future validations.

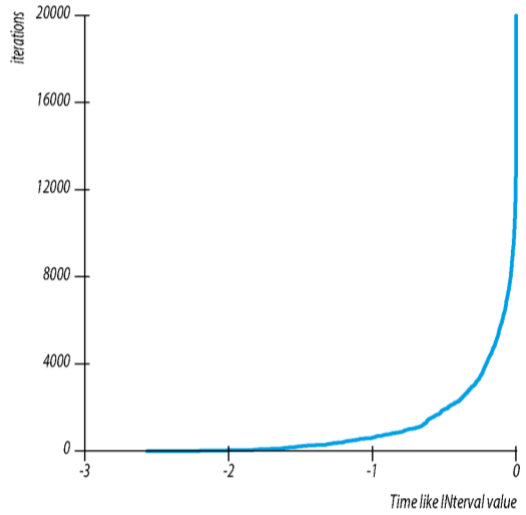

Figure 11. Illustration of the consistency of one time-like negative signature of one parameter space found in our simulations. This parameter space uniquely defined the dendrogramic space

we will demonstrate now that at least one of the consistent parameters with a "positive spacelike signature" have the ability to uniquely define a unique dendrogram structure (this set of z, z1, z2, z3, z4 and parameters θ'_1 , θ'_2 , θ'_3 *and* θ'_4 are the one shown as examples in figures 6 and 10).

$$\theta'_1 = (U_D)^{-2}$$
$$\theta'_2 = (V_D)^{0.5}/(U_D)^{-2}$$
$$\theta'_3 = (U_D)^{-2}(V_D)^{0.5}{R_D}^{-0.5}(M_D)^2$$
$$\theta'_4 = \sqrt{n}(r_D)^2/{R_D}^{-0.5}$$

Let's suppose $\theta'_1 = \theta''_1$, $\theta'_2 = \theta''_2$, $\theta'_3 = \theta''_3$ *and* $\theta'_4 = \theta''_4$ *for two different dendrograms* D' *and* D'' *then if* $\theta'_1 = \theta''_1$ *and* $\theta'_2 = \theta''_2$ *then* $(U_{D'})^{-2} = (U_{D''})^{-2}$ *and* $\frac{(V_{D'})^{0.5}}{(U_{D'})^{-2}} = \frac{(V_{D''})^{0.5}}{(U_{D''})^{-2}}$ *which means* $(V_{D'})^{0.5} = (V_{D''})^{0.5}$ *the combination*

$\begin{cases}(U_{D'})^{-2} = (U_{D''})^{-2} \\ (U_{D'})^{-2} = (U_{D''})^{-2}\end{cases}$ *can't happen by their definition unless* $D' = D''$ *and we are done.*

Now for the consequence of our numerical analysis. We propose that

$$p_{\theta'}(X) = \frac{1}{(2\pi a^2)^2}\exp\left(-\frac{(t - i(s2)\theta'_4)^2 + (x - \theta'_1)^2 + (y - \theta'_2)^2 + (z - \theta'_3)^2}{2a^2}\right)$$

Where X is a vector of [t,x,y,z] and s2 is our equivalent of c=speed of light and is defined above in equation 6.

this distribution is normalized: meaning $\int d^4x\, p_{\theta'}(X) = 1$
and leads to

the following fisher information matrix $g_{\mu\nu} = \begin{pmatrix} -s2 & 0 & 0 & 0 \\ 0 & 1 & 0 & 0 \\ 0 & 0 & 1 & 0 \\ 0 & 0 & 0 & 1 \end{pmatrix}$

After rescaling by a^2 [16].
Furthermore, we define *n=number of events in dendrogram 1, n'=number of events in dendrogram 2,*
N=|n-n'| and we define the simultaneity matrix or operator for the positive signature space like combinations

$$\widehat{sym_+} = \begin{pmatrix} \lceil \frac{N}{N+1} \rceil & 0 & 0 & 0 \\ 0 & 1 & 0 & 0 \\ 0 & 0 & 1 & 0 \\ 0 & 0 & 0 & 1 \end{pmatrix}$$

$$dist(dendrogram1, dendrogram2) = \widehat{(sym_+)}_{\mu\nu} g_{\mu\nu} d\theta'_\mu d\theta'_\nu$$

One benefit of this construction is the transformation of the discrete parameter space into a continuous one. Thus, every dendrogram is defined by its non-hermitian distribution $p_{\theta'}(X)$ defined above (ref) and we operate on a smooth Riemann 4d parameter space. In that way, we can also find the null-like parameters for a given dendrogram (although they will (probably) not represent a dendrogram)

5. The informational Minkowski-like metric of the dendrogramic space

Having established the existence of spaces with four parameters that uniquely determine a dendrogram, we can now develop an informational metric inspired by Minkowski spacetime. We will describe our model step by step: each parameter point in parameter space uniquely defines a dendrogram. This dendrogram is the n-level state of an ensemble of observers with the same dendrogram (note that in the numerical study above we constructed the same initial dendrogram for 100 different sets of n random numbers). Thus, such a point in parameter space has a flow-in of observers from a distribution of observers on θ' **of** lower-level parameter points (the past of that point).

Furthermore, the dendrogram at level n exhibits a flow of observers emanating from this parameter point, where the ensemble of observers is distributed to the next level in a certain manner, representing the future distribution of the n-level point. Specifically, for a single dendrogram at level n, its future cone at level n+k (where k ranges from 1 to M→∞) displays k distributions $\rho_{k,n}(\theta')_{future}$, dependent on the level of the initial point in the parameter space as well as the particular θ' at that level n. Similarly, the past cone of a dendrogram at level n extends to level n-k (where k ranges from 1 to n-2) and exhibits k distributions $\rho_{k,n}(\theta')_{past}$ (see Figure 6).

It is noteworthy that, as k approaches infinity, the distributions tend to flatten, such that at infinity each observer acquires a unique infinite dendrogram. Therefore, at infinity, the particular point θ'' has a distribution of 1/N (where N is the number of

observers), as each observer possesses a unique dendrogram. The subset of all infinite dendrograms belonging to the point θ' defines θ', and vice versa. Consequently, if there exists an intersection between the infinite dendrograms associated with $\theta'1$ and $\theta'2$, it implies that there are observers flowing from one point to the other, establishing a causal connection or indicating a timelike separation between the two parameters. On the other hand, if the intersection is an empty set, it signifies a spacelike separation between the two parameters.

We conclude by stressing that a point in parameter space is accompanied by all its past distributions flowing into that point and all future distributions flowing out of that point and both the distributions and the point are defined by the set of observers that flow in and out of that point set of ultimate infinite dendrograms and vice versa (figure 12). These distribution dynamics are manifested from level to level by a "potential"/"force" we call the "Leibnitz potential/force" which forces the observers to become distinct (ultimately at the ontic infinite sub-dendrogram). Otherwise, the Leibnitz principle holds where:

Leibniz's principle (identity of indiscernibles) states that If, for every property F, object x has F if and only if object y has F, then x is identical to y. In our case, it translates to If, for every dendrogram D_∞, observer x has D_∞ if and only if observer y has D_∞, then observer x is identical to observer y.

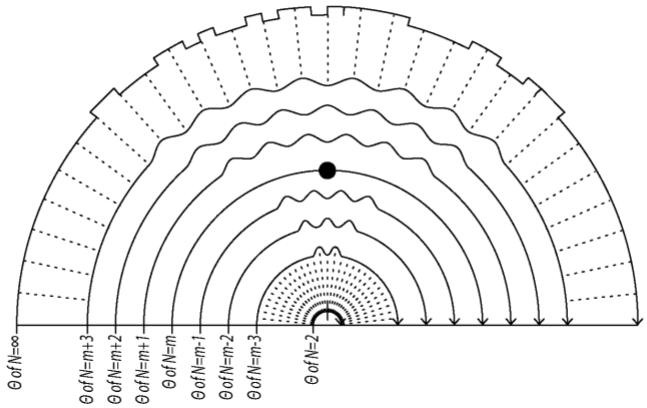

Figure 12. Representation of a point in the dendrogramic parameter space and its accompanied distributions in each of the future and past levels.

This is an infect the ontic realization of Leibnitz principle.

To quantify the informational distance between two parameter points accompanied by their distribution, we propose a metric:

$$informational\ distance = 2H_f^{\lceil T \rceil} + 2H_p^{\lceil T \rceil} - \left(H_{f'} + H_{p'}\right) - 2\left(\frac{L}{L+1}H_{ratio} + \lceil T \rceil\right)$$

Consider two points $\theta'1$ *and* $\theta'2$ *and* $n1, n2$ *are their level where without loss of generality* $n1 \leq n2$*:*

H_f =*Hellinger distance between* $\rho_{k,n1,\theta'1}(x)_{future\ at\ n2+1}$ *and* $\rho_{k,n2,\theta'2}(x)_{future\ at\ n2+1}$ *(see figure 13), if* $\rho_{k,n1,\theta'1}(x)_{future\ at\ n2+1}$ *and* $\rho_{k,n2,\theta'2}(x)_{future\ at\ n2+1}$ *share parameter points with non-zero probability* $0 \leq H_f < 1$ *else* $H_f = 1$

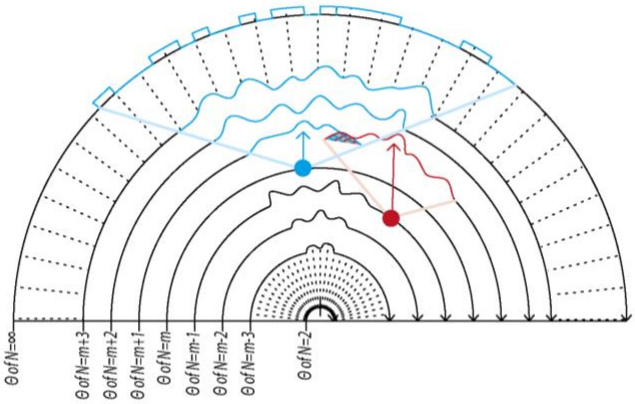

Figure 13. Representation of the H_f =*Hellinger distance between* $\rho_{k,n1,\theta'1}(x)_{future\ at\ n2+1}$ *and* $\rho_{k,n2,\theta'2}(x)_{future\ at\ n2+1}$

H_p =*Hellinger distance between* $\rho_{k,n1,\theta'1}(x)_{past\ at\ n1-1}$ *and* $\rho_{k,n2,\theta'2}(x)_{past\ at\ n1-1}$ *(see figure 14), if* $\rho_{k,n1,\theta'1}(x)_{past\ at\ n1-1}$ *and* $\rho_{k,n2,\theta'2}(x)_{past\ at\ n1-1}$ *share parameter points with non-zero probability* $0 \leq H_f < 1$ *else* $H_f = 1$

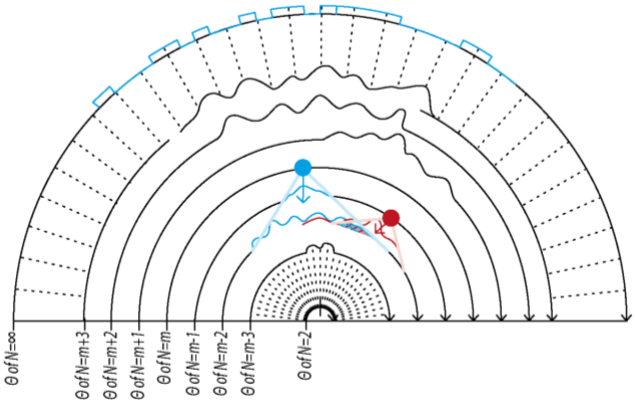

Figure 14. Representation of the H_p =*Hellinger distance between* $\rho_{k,n1,\theta'1}(x)_{past\ at\ n1-1}$ *and* $\rho_{k,n2,\theta'2}(x)_{past\ at\ n1-1}$

$\rho_{k,\overset{\cdots}{n1},\theta'1}(x)_{\ future\ n1+k1}$ = *lowest k1 value distribution of* $\theta'1$ *that shares parameter points with non zero probability, lowest k2 value with* $\rho_{k,n2,\theta'2}(x)_{future\ n2+k2}$. *Thus:*
$H_{f'}$ =*Hellinger distance between* $\rho_{k,\overset{\cdots}{n1},\theta'1}(x)_{\ future\ n1+k1}$ *and* $\rho_{k,n2,\theta'2}(x)_{future\ n2+k2}$ *(figure 15)*

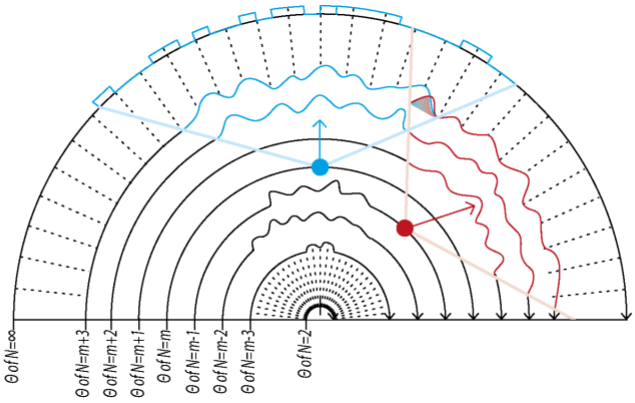

Figure 15. Representation of the H_f, =*Hellinger distance between* $\rho_{k,\vec{n1},\theta'1}(x)_{\ future\ n1+k1}$ *and* $\rho_{k,n2,\theta'2}(x)_{future\ n2+k2}$

$\rho_{k,\vec{n2},\theta'2}(x)_{\ past\ n2-k2}$ = *lowest k2 value distribution of* $\theta'2$ *that shares parameter points, with non zero probability, with lowest k1 value distribution* $\rho_{k,n1,\theta'1}(x)_{past\ n1-k1}$. *Thus:* H_p, =*Hellinger distance between* $\rho_{k,\vec{n2},\theta'2}(x)_{\ past\ n2-k2}$ *and* $\rho_{k,n1,\theta'1}(x)_{past\ n1-k1}$ *(figure16)*

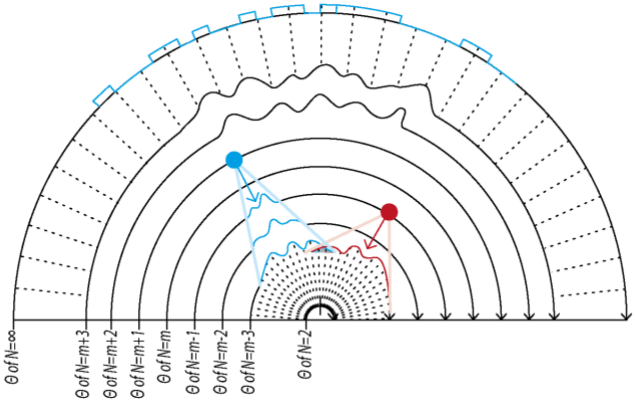

Figure 16. Representation of the H_p, =*Hellinger distance between* $\rho_{k,\vec{n2},\theta'2}(x)_{\ past\ n2-k2}$ *and* $\rho_{k,n1,\theta'1}(x)_{past\ n1-k1}$

$$L = |n1 - n2|$$

H_{ratio} = *Hellinger distance of two distributions* $p_{pop\ \theta'1}$ *and* $p_{pop\ \theta'2}$

Where $p_{pop\ \theta'1} =$

$$[\frac{number\ of\ observers\ at\ point\ \theta'1\ at\ lenvel\ n1}{total\ number\ of\ observers}\ \frac{number\ of\ observers\ at\ points\ other\ then\ \theta'1\ at\ level\ n1}{total\ number\ of\ observers}]$$

$p_{pop\ \theta'1}$

$$= [\frac{number\ of\ observers\ at\ point\ \theta'2\ at\ level\ n2}{total\ number\ of\ observers}\ \frac{number\ of\ observers\ at\ points\ other\ then\ \theta'2\ at}{total\ number\ of\ observers}$$

$T = p_{\theta'1}(x = \theta'2)$ =*distribution value of* $\rho_{k,n1,\theta'1}(x)_{future\ at\ n2}$ *at* $x=\theta'2$ *see figure 17.*

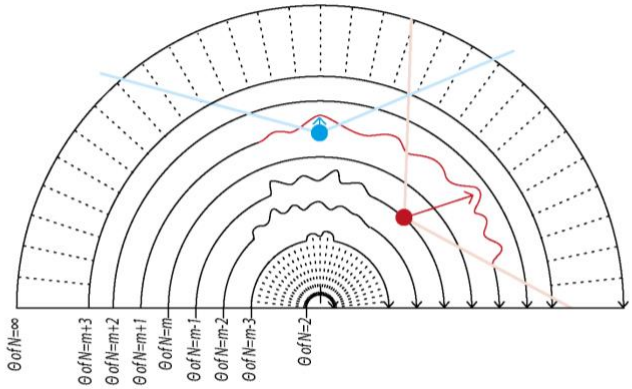

Figure 17. Representation of $T = p_{\theta'1}(x = \theta'2)$ =*distribution value of* $\rho_{k,n1,\theta'1}(x)_{future\ at\ n2}$ *at* $x=\theta'2$

Now for proving the timelike/spacelike signature:
For time like dendrograms H_f=$H_{f'}$, $H_p = H_{p'}$ and $\lceil T \rceil = 1$. Thus, the metric reduces to:
$informational\ distance = H_f + H_p - 2\left(\frac{L}{L+1}H_{ratio} + \lceil T \rceil\right)$.
$0 \le H_f + H_p < 2$ since they are timelike. On the other hand: $H_{ratio} \le 1$, $\frac{L}{L+1} < 1$
As $\lceil p_{\theta'1}(x = \theta'2)\rceil = \lceil T \rceil = 1$ as in timelike dendrograms some fraction of observer flow from one dendrogram to the other.
So, the component $2 \le 2\left(\frac{L}{L+1}H_{ratio} + \lceil T \rceil\right)$ resulting in:

$$H_f + H_p - 2\left(\frac{L}{L+1}H_{ratio} + \lceil T \rceil\right) < 0$$

Now for space-like, we have in fact two cases let's treat the first one where n1<n2
$H_f = 1, H_p = 1$, thus, we reduce the metric to $4 - (H_{f'} + H_{p'}) - 2\left(\frac{L}{L+1}H_{ratio} + \lceil T \rceil\right)$.

$$0 < (H_{f'} + H_{p'}) \le 2 \rightarrow\ 4 - (H_{f'} + H_{p'}) \ge 2$$

Then for $2\left(\frac{L}{L+1}H_{ratio} + \lceil T \rceil\right)$ we have again $H_{ratio} \le 1$, $\frac{L}{L+1} < 1$ but $\lceil p_{\theta'1}(x = \theta'2)\rceil = \lceil T \rceil = 0$ so $2\left(\frac{L}{L+1}H_{ratio} + \lceil T \rceil\right) < 2$

The other case is when $H_f < 1, H_p < 1$ then H_f=$H_{f'}$, $H_p = H_{p'}$ and $\lceil T \rceil = 0$ leading to

$$informational\ distance = 4 - (H_f + H_p) - 2\left(\frac{L}{L+1}H_{ratio} + \lceil T \rceil\right)$$

Again $0 \le H_f + H_p < 2$ thus $4 - (H_{f'} + H_{p'}) \ge 2$ but $2\left(\frac{L}{L+1}H_{ratio} + \lceil T \rceil\right)$ reduces to

$$2\left(\frac{L}{L+1}H_{ratio}\right) < 2$$

Thus: $4 - (H_{f'} + H_{p'}) - 2\left(\frac{L}{L+1}H_{ratio} + \lceil T \rceil\right) > 0$

For n1=n2

We have if $H_f = 1, H_p = 1 \longrightarrow\ 4 - (H_{f'} + H_{p'}) - 2\left(\frac{L}{L+1} H_{ratio} + \lceil T \rceil\right)$ since $\lceil T \rceil = 0$ and $L = 0$ thus $2\left(\frac{L}{L+1} H_{ratio} + \lceil T \rceil\right)$=0 and we have $4 - (H_{f'} + H_{p'}) \geq 2$
And we are done

If We have if $H_f < 1, H_p < 1 \longrightarrow\ 4 - (H_{f'} + H_{p'}) - 2\left(\frac{L}{L+1} H_{ratio} + \lceil T \rceil\right)$ since $\lceil T \rceil = 0$ and $L = 0$ where H_f=$H_{f'}$, $H_p = H_{p'}$ we conclude that $2\left(\frac{L}{L+1} H_{ratio} + \lceil T \rceil\right)$=0 and we have $4 - (H_{f'} + H_{p'}) \geq 2$
And we are done.

6. Concluding remarks

Exploring the treelike geometry opens a new direction in the modelling of the event universe endowed with a hierarchic relational structure. At the epistemic level, experimental data collected by an observer is represented with the aid of a clustering algorithm by a dendrogram – a finite tree. The collection of new data restructures the observer's dendrogram. Such dynamical restructuring is nonlocal w.r.t. the hierarchic relation between events: the appearance of a new event restructures the whole dendrogram. As we know relational mechanics and event universe play an important role in the modern development of quantum foundations [[17–24]]. Our approach, DHT [[1–8]], gives new mathematical and physical insights to this area of research. Of course, it is important to connect relational event physical models with conventional models based on the real space-time endowed with Minkowski's causal structure. In the present paper, we proceed in this direction. We start with an introduction to the causal structure of the dendrogramic configuration space. This causality is statistical and reflects dendrogramic dynamics for ensembles of observers. This is a novel approach to causality. Then we encode dendrograms by real parameters. This gives the possibility to determine the four-dimensional real space-time and information geometry on it matching the statistical observers' causality. Via this construction, transformations of special relativity can be realized in the dendrogramic configuration space. This is the topic for the further development of DHT.

Finally, we remark once again that DHT finds applications outside of physics, in the modelling of information processing by the brain and medical diagnostics of the brain disorders. The method developed in the present paper gives the possibility to invent a kind of Minkowski causal structure on the mental space. In future studies, we shall employ this structure for medical diagnostics.

References:

[1] Shor, O., Benninger, F., & Khrennikov, A. (2021). Representation of the universe as a dendrogramic hologram endowed with relational interpretation. *Entropy, 23*.

[2] Shor, O., Benninger, F., & Khrennikov, A. (2021). Dendrogramic representation of data: Chsh violation vs. nonergodicity. *Entropy, 23*.

[3] Shor, O., Benninger, F., & Khrennikov, A. (2022). Towards unification of general relativity and quantum theory: Dendrogram representation of the event-universe. *Entropy, 24*.

[4] Shor, O., Benninger, F., & Khrennikov, A. (2022). Dendrographic hologram theory: Predictability of relational dynamics of the event universe and the emergence of time arrow. *Symmetry (Basel), 14*.
[5] Shor, O., Benninger, F., & Khrennikov, A. (2022). Emergent quantum mechanics of the event-universe, quantization of events via dendrographic hologram theory. arXiv preprint arXiv:2208.01931.
[6] Shor, O., Benninger, F., & Khrennikov, A. Rao-Fisher information geometry and dynamics of the event-universe views distributions.
[7] Shor, O., Glik, A., Yaniv-Rosenfeld, A., Valevski, A., Weizman, A., Khrennikov, A., & Benninger, F. (2021). EEG p-adic quantum potential accurately identifies depression, schizophrenia and cognitive decline. *PLoS One, 16*, e0255529.
[8] Shor, O., Yaniv-Rosenfeld, A., Valevski, A., Weizman, A., Khrennikov, A., & Benninger, F. (2023). EEG-based spatio-temporal relation signatures for the diagnosis of depression and schizophrenia. *Sci Rep, 13*, 776.
[9] Vladimirov, V.S., Volovich, I.V., & Zelenov, E.I. (1994). P-adic analysis and mathematical physics. World Scientific, Singapore.
[10] Volovich, I.V. (1987). p-adic string. *Class. Quantum Gravity, 4*, 83–87.
[11] Volovich, I.V. (2010). Number theory as the ultimate physical theory. *P-Adic Numbers, Ultrametric Analysis, and Applications, 2*, 77–87.
[12] Aref'eva, I. Ya., Dragovich, B., Frampton, P. H., & Volovich, I.V. The wave function of the universe and p-adic gravity. *Int. J. Mod. Phys A, 6*, 4341–4358.
[13] Freund, P.G.O., & Witten, E. (1987). Adelic string amplitudes. *Physics Letters B, 199*, 191–4.
[14] Parisi, G. (1988). On p-adic functional integrals. *Mod Phys Lett A, 3*, 639–43.
[15] Parisi, G., & Sourlas, N. (2000). P-adic numbers and replica symmetry breaking. *The European Physical Journal B - Condensed Matter and Complex Systems, 14*, 535–42.
[16] Calmet, J., & Calmet, X. (2004). Metric on a statistical space-time. arXiv preprint math-ph/0403043.
[17] Rovelli, C. (1996). Relational quantum mechanics. *International Journal of Theoretical Physics, 35*, 1637–78.
[18] Rovelli, C., Segre, E., & Carnell, S. (2018). The order of time. Penguin Books Limited.
[19] Smolin, L. (2019). Einstein's unfinished revolution: The search for what lies beyond the quantum.
[20] Smolin, L. (2016). Quantum mechanics and the principle of maximal variety. *Found Phys, 46*, 736–58.
[21] Smolin, L. (2018). The dynamics of difference. *Found Phys, 48*, 121–34.
[22] Cortês, M., & Smolin, L. (2014). The universe as a process of unique events. *Physical Review D - Particles, Fields, Gravitation and Cosmology, 90*, 1–30.
[23] Barbour, J., & Smolin, L. (1992). Extremal variety as the foundation of a cosmological quantum theory, 1–35.
[24] Barbour, J., Koslowski, T., & Mercati, F. (2014). Identification of a gravitational arrow of time. *Phys Rev Lett, 113*, 181101.